



Diagnostic Imaging of Gastrointestinal Stromal Tumor

4

Tomohiro Yoneyama, Bae Hyeyeol, Yoshio Kitazume, Mitsuhiro Kishino, and Ukihide Tateishi

Abstract

GIST is the most frequent mesenchymal tumor in the digestive tract. Imaging modalities comprising of ultrasound, computed tomography (CT), magnetic resonance imaging (MRI), and positron emission tomography/computed tomography (PET/CT) are routinely used for management of tumor. We focus on diagnosis of staging, recurrence, and monitoring.

Keywords

GIST · Imaging · CT · MRI · PET/CT

4.1 Introduction

In 1983, Mazur and Clark defined the gastrointestinal stromal tumor (GIST) as a characteristic subgroup of gastrointestinal mesenchymal tumors unclassified as deriving from neural or smooth muscle [1]. Kindblom et al. hypothesized that these tumors may arise from Kahal's stromal cells in the normal intestinal plexus [2]. This hypothesis was confirmed by Hirota et al. in 2000 [3]. Nowadays, based on pathological features, GIST is defined as a mesenchymal tumor of the gastrointestinal tract that expresses positive for KIT (CD117), the c-kit receptor tyrosine kinase.

T. Yoneyama · B. Hyeyeol · Y. Kitazume · M. Kishino · U. Tateishi (✉)
Department of Diagnostic Radiology, Tokyo Medical and Dental University, Tokyo, Japan
e-mail: ttisdrmm@tmd.ac.jp

GIST is the most frequent mesenchymal tumor in the digestive tract. Despite accounting for only about 3% of all malignant tumors of the stomach, GIST is the most frequent in malignant tumors of small bowel and accounts for 20%. It occurs in the stomach (60–70%), small intestine (20–25%), rectum, esophagus, colon, and appendix.

Approximately 95% of GIST is positive for KIT. The mutation of KIT leads to activation with the receptor dimerization independent of the ligand of KIT tyrosine kinase. These mutations are confirmed in more than 80% of GIST, and most of the mutations occur in the vicinity of the membrane encoded by exon 11. Mutations may also occur at exons 9, 13, 17 or platelet-derived growth factor receptor (PDGFR). At a response rate of 85%, they show significant clinical response to imatinib therapy. Sunitinib therapy is the second molecular-target therapy, which is a multi-target tyrosine kinase inhibitor of KIT and PDGFR.

Most of GISTs can be diagnosed on KIT immunoreactivity. However, some neoplasms show weak or negative KIT expression [4]. They are very rare, accounting for less than 5% of all GISTs [5] and usually occur in the stomach, omentum, or mesentery. The cytogenetic analysis revealed the existence of mutations of the platelet-derived growth factor receptor α (PDGFRA) gene which was also the product of the c-kit proto-oncogene in KIT-weak or KIT-negative GISTs [6].

4.2 Staging

Staging of GIST differs between gastric GIST and small intestinal GIST. In stage I–III, both gastric GIST and small intestinal GIST are classified in accordance with the size of tumor and mitotic rate (histologic grade).

4.2.1 Staging of Gastric GIST

Stage I is divided into stage I,A and stage I,B, depending on the size of tumor in the greatest dimension under the condition of mitotic rate 5/50 per high-power field (HPF) or less. Stage I,A: the size of tumor is not more than 5 cm. Stage I,B: the size of tumor is more than 5 cm but not more than 10 cm. In stage II, the size of tumor in greatest dimension is more than 10 cm under the condition of mitotic rate 5/50 per HPF or less, or the size of tumor is not more than 5 cm under the condition of mitotic rate >5/50 HPF. Stage III is divided into stage III,A and stage III,B depending on the size of tumor in the greatest dimension under the condition of mitotic rate >5/50 HPF. Stage III,A: the size of tumor is more than 5 cm but not more than 10 cm. Stage III,B: the size of tumor is more than 10 cm. In stage IV, gastric GIST has at least one lymph node metastasis and/or distant metastasis regardless of the size of tumor and mitotic rate.

4.2.2 Staging of Small Intestinal GIST

In stage I, the size of tumor in greatest dimension is not more than 5 cm under the condition of mitotic rate 5/50 per HPF or less. In stage II, the size of tumor in greatest dimension is more than 5 cm but not more than 10 cm under the same condition. Stage III is divided into stage III,A and stage III,B, depending on the size of tumor in greatest dimension and mitotic rate. Stage III,A: the size of tumor is more than 10 cm under the condition of mitotic rate 5/50 per HPF or less. Stage III,B: the size of tumor is more than 2 cm but not more than 10 cm under the condition of mitotic rate >5/50 HPF. In stage IV, small intestinal GIST has at least one lymph node metastasis and/or distant metastasis regardless of the size of tumor and mitotic rate.

4.3 Primary Tumor

Computed tomography (CT) and magnetic resonance imaging (MRI) are well-accepted methods for diagnosis and staging of GISTs [7–11].

4.3.1 CT

CT allows precise assessment of tumor morphology, composition, location, and extent. Relevant anatomy is well visualized on axial, coronal, and sagittal images as well as any oblique planes provided by multiplanar reconstruction or reformatting. CT features of GIST show various findings depending on the size and aggressiveness of the tumor [12, 13]. On unenhanced CT, GISTs typically show isodense to normal muscle, and enhancing masses on contrast-enhanced CT (Fig. 4.1). Heterogeneous enhancements are often observed because of necrosis, hemorrhage, or cystic degeneration [7–11]. Intralesional calcifications are sometimes confirmed as clinicopathologic feature of GISTs and CT is superior to MRI in detecting them. The calcifications within GISTs distribute circumscribed and patchy. They are thought to be caused by previous bleeding or tumor necrosis with cystic degeneration [8]. Time density curve of contrast-enhanced CT demonstrates optimal timing of scan delay (Fig. 4.2). Dynamic contrast-enhanced CT images provides information of tumor vascularity and blood flow; i.e., k1–k4 and areas under the curve (AUC), being calculated by two- or three-compartment model.

GISTs usually oppress and displace adjacent structures, and the direct invasion is sometimes observed with advanced disease. In the case of large GIST, the origin is difficult to be identified due to its prominent extraluminal location. Small GISTs usually show endoluminal and polypoid appearance, and are homogenous.

Tateishi et al. reported that the CT findings, including lesion larger than 11.1 cm, irregular surface, unclear boundary, presence of invasion, heterogeneous enhancement, hepatic metastasis, and peritoneal dissemination, were more

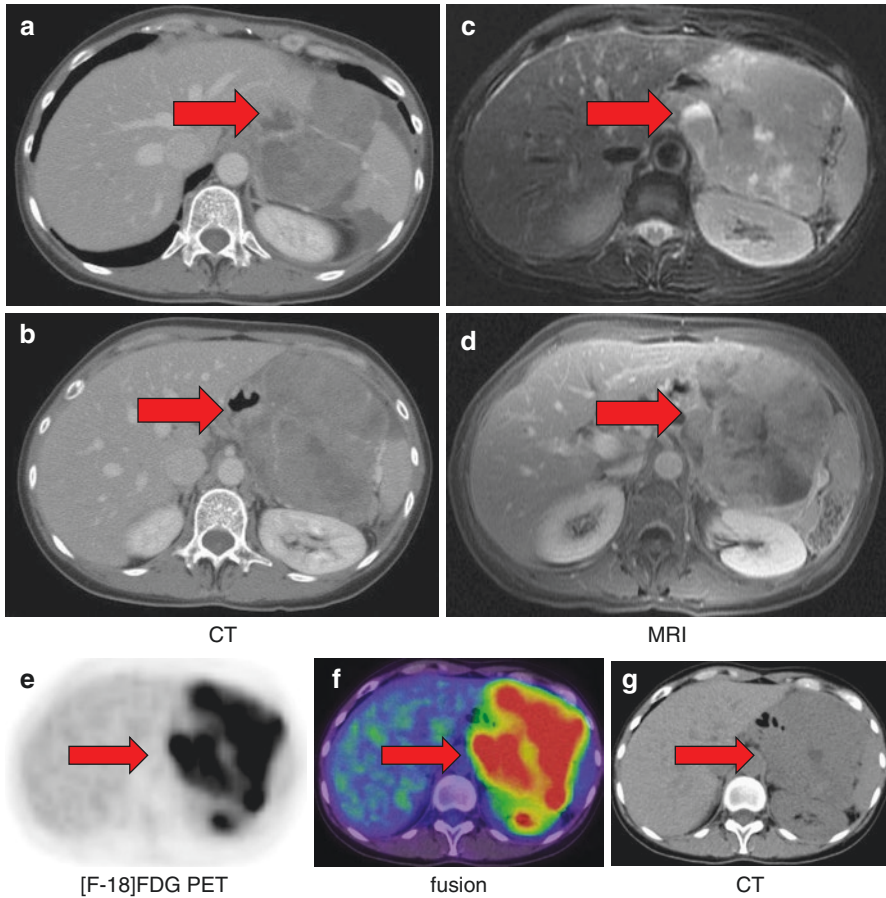


Fig. 4.1 A man of 50 years with gastric GIST. Tumor greater than 11 cm in the long axis demonstrates heterogeneous enhancement on axial contrast-enhanced CT (**a, b**: arrow). Axial T2-weighted MR image shows heterogeneous hypersignal intensity relative to muscle (**c**, arrow). Tumor shows heterogeneous enhancement on gadolinium-enhanced T1-weighted MR image (**d**, arrow). [F-18] FDG PET/CT reveals high avidity of tumor (**e-g**, arrow)

often found in high-grade GISTs and were associated significantly with decreased survival. Especially, a lesion larger than 11.1 cm, wall invasion of the target organ, and hepatic metastasis identified on CT images had a significant effect on prognosis [14].

4.3.2 MRI

MRI allows tissue characterization, accurate assessment of tumor extent, differentiation from structures, information of blood flow, diffusion capacity,

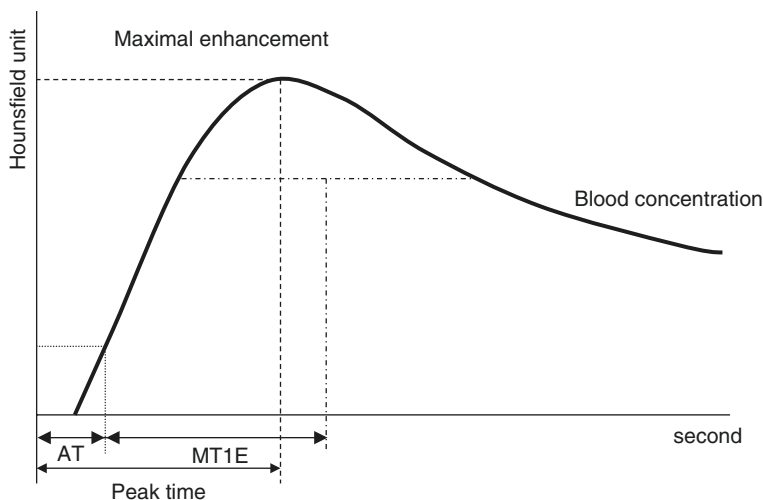


Fig. 4.2 Time density curve after administration of contrast media on CT. The curve shows maximal density at peak time after intravenous administration of contrast media. After delayed phase, tumor density decreases to blood concentration. *AT* appearance time of contrast media, *MTIE* mean transit time of enhancement

texture features, and specification of metabolites within tumors. On unenhanced MRI, GISTs appear as isointense to normal muscle on T1-weighted images and hyperintense on T2-weighted images, and moderately or mildly enhanced. Reflecting intralesional necrosis or hemorrhage, a heterogeneous pattern of enhancement is more common on contrast-enhanced MRI, similar to CT (Fig. 4.1). Following MRI findings must be collected for differentiation of tumor: tumor size, location, types of margin and contours, internal architecture, tumor capsule, signal characteristics, and heterogeneity. On gadolinium contrast-enhanced studies, the extent (none/weak or pronounced), pattern (punctate or diffuse), and homogeneity after administration are also recorded for assessment. However, gadolinium enhancement pattern of GIST is similar to those of contrast-enhanced CT.

Yu et al. reported that the features of small GISTs were round shape with a homogeneous enhancement pattern, and large GISTs had a lobulated shape, heterogeneous enhancement pattern, and intratumoral cystic change [15]. They also found that the prevalence of intratumoral cystic change was significantly higher in the moderate to high risk group than in the very low to low risk group, and the intratumoral cystic change seen on MR images correlated with tumor necrosis, hemorrhage at pathologic examination. Atypical GIST with KIT-weak or KIT-negative often showed a large extraluminal mass with heterogeneous lesion containing cystic regions and soft tissue elements in CT and MRI images. However, it is impossible to diagnose atypical GISTs from conventional GISTs, because these findings are not specific [16].

4.3.3 Positron Emission Tomography/Computed Tomography (PET/CT)

Functional imaging methods, especially [F-18] fluorodeoxyglucose—positron emission tomography/computed tomography ([F-18] FDG -PET/CT), had played a pivotal role in the management of GIST, which can provide the information of metabolic activity in addition to morphologic features (Fig. 4.1). The uptake of GIST exhibits various patterns and intensity in PET/CT with [F-18] FDG. Malignant cells are frequently associated with increased metabolic activity. [F-18] FDG, which accumulates in proportion to the glucose metabolism, is the PET tracer most commonly used in oncology. [F-18] FDG uptake is generally higher in malignant lesions than benign ones, while it is also seen in inflammatory changes or fractures. Miyake et al. classified the uptake pattern of GIST into four patterns (“Ring-shaped” was defined as round or semi-round uptake with an apparent central uptake defect, “Homogeneous/diffuse” was defined as fairly uniform uptake covering almost the entire tumor, “Heterogeneous/partial” was defined as inhomogeneous or deficient uptake, and other than above is “unclassified”) and scored the uptake intensity on a four-point scale (“faint-to-none” for uptake less than background hepatic uptake, “mild” for uptake similar to liver uptake, “moderate” for uptake moderately greater than hepatic uptake, and “intense” for intense uptake equal to or greater than brain uptake). Then, they investigated the correlation between the uptake pattern or uptake intensity and recurrence-free survival (RFS). As a result, ring-shaped uptake was significantly associated with lower RFS compared to those with the other uptake patterns. Intense uptake also had a significant association with lower RFS [17]. Recently, PET/MRI has been introduced and used in the assessment of malignancies including GIST. [F-18] FDG PET/MRI possesses highly diagnostic performance. MRI also provides the reduction of radiation exposure, especially pivotal in younger patients. However, PET/MRI has the disadvantages of longer examination times, the difficulty in evaluating lung lesions and metallic artifacts.

4.4 Metastases

The most common metastatic site is liver, detected in 70% of patients followed by the peritoneum, whereas, bone, lung, and lymph nodes are low frequency as a site of metastasis [13, 18]. Liver metastases show various appearances that resemble primary lesions. On CT images, they are often multiple and appear low density mass with peripheral enhancement reflecting necrosis at the center and peripheral solid component. Enhancement pattern on CT depends on scan delay after intravenous administration of contrast agent. When we stratify by hepatic metastasis of GIST, hepatic blood flow affects flow-through pattern of contrast medium. Patterns of contrast enhancement depend on flow-through pattern (Figs. 4.3 and 4.4). Therefore, optimal timing has to be determined in order to detect more precisely based on time density curve (Fig. 4.2). Metastasis sometimes shows the variegated appearance due to protein material, bleeding, and calcification [19]. Although

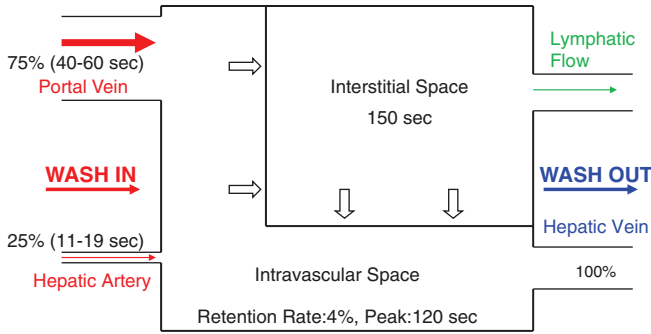


Fig. 4.3 Schematic compartmental model of contrast medium flow-through pattern. Hepatic inflow consists of portal vein and hepatic artery as wash-in. Administered contrast media reaches to liver mostly via portal vein at 40–60 s. Contrast media doesn't retain intravascular space and move to interstitial space at 150 s. Finally, out-flow consists of hepatic vein and lymphatic vessels as wash-out

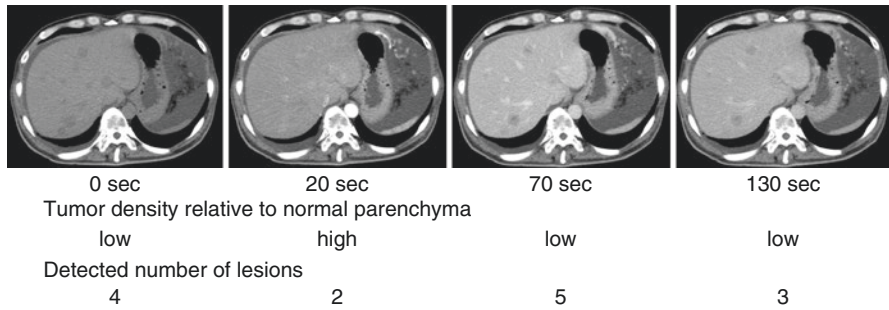


Fig. 4.4 Dynamic contrast-enhanced CT series in a man of 60 years with hepatic metastases of GIST. Visual assessment of tumor density relative to normal parenchyma and the numbers of detected hepatic metastases are presented. Image obtained at 70 s reveals maximal number of lesions compared to other phases. Optimal CT timing is important to assess hepatic metastasis of GIST on dynamic contrast-enhanced CT

gadolinium enhancement pattern of GIST is similar to those of contrast-enhanced CT, MRI using super paramagnetic iron oxide (SPIO) provides us to visualize metastatic liver tumor. SPIO is usually distributed in blood and Kupffer cell after intravenous administration. Hepatic metastasis is hypersignal relative to adjacent normal liver tissue on T2-weighted MR images. Hepatocyte specific contrast agent has been used for differentiation from hepatocellular carcinoma. Peritoneal lesions often show large discrete masses that appear similar to the primary tumor. Most of the peritoneal spread is caused by the tumor seedling during surgery and biopsy [20].

The lymph node metastases of GIST patients are believed to be 1–4% [21, 22]. However, pediatric and young adult patients have higher frequency. Agaimy and Peter reported that the lymph node metastases were observed in approximately 20% of patients ≤ 40 years. In addition, the frequency of lymph node metastasis varies

depending on the primary site [23]. Gong et al. reported that the most notable factor of the lymph node metastasis is the location of the primary tumor. Out of five adult patients, four patients' primary tumors were located at very uncommon places as prostate, duodenum, right ovary, and esophagus, only one is in stomach [24].

Gayed et al. compared the performance (true-positive, true-negative, false-positive, and false-negative findings) of [F-18] FDG PET and CT on the pretherapy scans. The sensitivity and positive predictive values were 93% and 100%, respectively, for CT and 86% and 98%, respectively, for [F-18] FDG PET. There was no statistical difference between CT and [F-18] FDG PET in the sensitivity or positive predictive values [25].

4.5 Monitoring Tumor Response

Conventional methods to monitor treatment response are based on the size reduction on CT. However, the changes of tumor metabolism often occur early during therapy and precede size reduction of the tumor. The quantification of tumor glucose metabolism is highly accurate for monitoring effects of chemotherapy. Choi et al. reported criteria based on contrast-enhanced CT with special reference to [F-18] FDG PET [26]. They suggested cutoff of tumor response with 10% change of maximal perpendicular diameter or 15% change of CT. However, change of CT density depends on scan delay, concentration of contrast media, bolus of contrast media, blood flow, and body weight (Fig. 4.5). The reduction of [F-18] FDG uptake

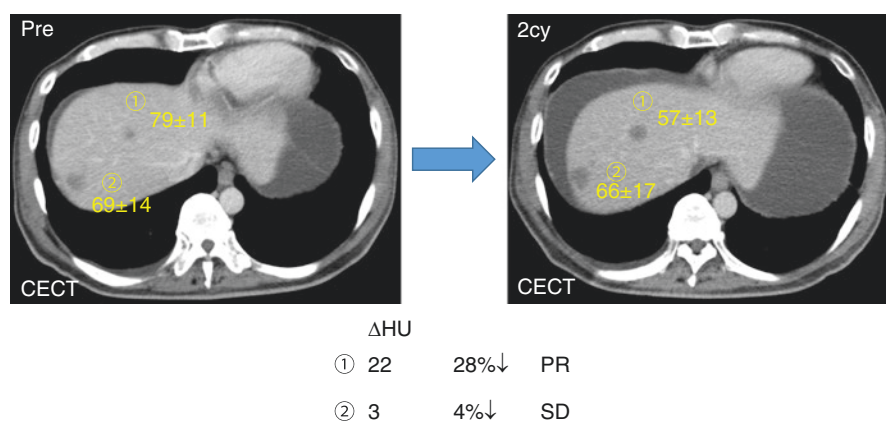
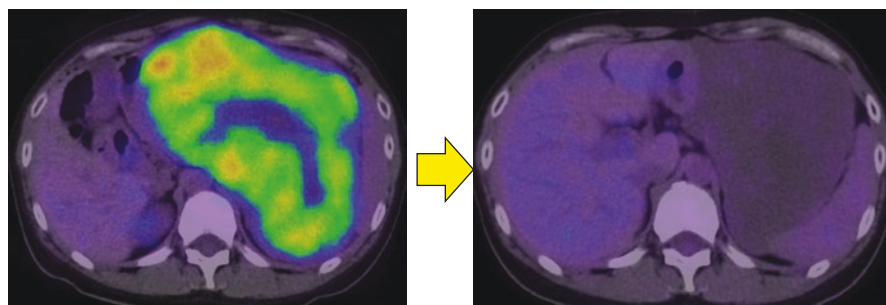


Fig. 4.5 Response assessment of two hepatic metastases on contrast-enhanced CT. One hepatic metastasis (①) shows 28% decrease of Hounsfield unit after 2 cycles of imatinib therapy and this lesion indicates partial response on Choi's criteria. In contrast, the other hepatic metastasis (②) demonstrates only 4% decrease of Hounsfield unit after 2 cycles of imatinib therapy with stable disease. Response assessment only by change of density has possibility to lead to inaccurate conclusion. General evaluation is needed for accurate response assessment. *Pre* baseline, *2cy* after 2 cycles, ΔHU change of Hounsfield unit, *PR* partial response, *SD* stable disease



	Day 0	Day 60
SUVmax, g/ml	11.3	1.9
TLG, g	6808	440
Size, mm	144.6	88.7
Volume, cm ³	1565	484

Fig. 4.6 Monitoring of response of gastric GIST. Typical responder shows parallel decrease in SUV, TLG, size, and volume during the course of disease. Metabolic response by [F-18] FDG PET/CT usually precedes morphometric changes of CT. *SUV* standardized uptake value, *TLG* total lesion glycolysis

between pre- and post-chemotherapy has a relationship with histological change, often prior to morphologic changes on conventional imaging (Fig. 4.6). Fuster et al. evaluated the role of [F-18] FDG PET in assessing 21 patients with locally advanced and/or metastatic GIST refractory to high-dose imatinib treated with doxorubicin. Of 21 patients, 6 patients had partial response by [F-18] FDG PET obtained after 2 months of treatment, 9 showed stable disease, and 6 showed progression of disease based on European Organization for Research and Treatment of Cancer (EORTC) criteria. There was a significant correlation between PET response and progression-free survival (PFS) [27].

Prior et al. assessed tumor metabolism with [F-18] FDG PET before and after the first 4 weeks of sunitinib therapy in 23 patients who received 1–12 cycles of sunitinib therapy (4 weeks of 50 mg/day, 2 weeks off). They evaluated treatment response with the percent change in maximal standardized uptake values (SUV). Using -25% and $+25\%$ thresholds for SUV variations from baseline, early [F-18] FDG PET response was stratified in partial response (PR), stable disease (SD), or progressive disease (PR). The median PFS rates were 29 weeks in PR, 16 weeks in SD, and 4 weeks in PR, respectively. Similarly, when a single [F-18] FDG PET positive/negative was considered after 4 weeks of sunitinib, the median PFS was 29 weeks for SUVs less than 8 g/mL versus 4 weeks for SUVs of 8 g/mL or greater. Multivariate analysis showed shorter PFS in patients who had higher residual SUVs and PFS was correlated with early [F-18] FDG PET metabolic response [28].

4.6 Conclusion

Despite computed tomography (CT) and magnetic resonance imaging (MRI) are well-accepted methods for diagnosis and staging of GISTs, the findings obtained from these modalities are not specific. However, several papers reported the CT and MRI features indicating a benign and malignant tendency.

Although GISTs also show non-specific findings on [F-18] FDG PET, it has a significant role in monitoring tumor response during imatinib and sunitinib therapy. The prognosis of GIST patients has a high correlation with the remnant and decrease of SUV values. Especially, it is useful to be able to evaluate tumor response to therapy at an early stage.

Acknowledgments This work was supported in part by grants from Scientific Research Expenses for Health and Welfare Programs, the Grant-in-Aid for Cancer Research from the Ministry of Health, Labor and Welfare, No. 15K09885, the Scientific Research Expenses for Health and Welfare Programs, No. 29-A-3 (Takashi Terauchi and Ukihide Tateishi: squad leaders), Practical Research for Innovative Cancer Control and Project Promoting Clinical Trials for Development of New Drugs by Japan Agency for Medical Research and Development (AMED).

References

1. Mazur MT, Clark HB. Gastric stromal tumors. Reappraisal of histogenesis. *Am J Surg Pathol.* 1983;7:507–19.
2. Kindblom LG, Remotti HE, Aldenborg F, et al. Gastrointestinal pacemaker cell tumor (GIPACT): gastrointestinal stromal tumors show phenotypic characteristics of the interstitial cells of Cajal. *Am J Pathol.* 1998;152:1259–69.
3. Hirota S, et al. Effects of loss-of-function and gain-of-function mutations of c-kit on the gastrointestinal tract. *J Gastroenterol.* 2000;35:75–9.
4. Subramanian S, West RB, Corless CL, et al. Gastrointestinal stromal tumors (GISTs) with KIT and PDGFRA mutations have distinct gene expression profiles. *Oncogene.* 2004;23:7780.
5. Sakurai S, Hasegawa T, Sakuma Y, et al. Myxoid epithelioid gastrointestinal stromal tumor (GIST) with mast cell infiltrations: a subtype of GIST with mutations of platelet-derived growth factor receptor alpha gene. *Hum Pathol.* 2004;35:1223–30.
6. Hirota S, Ohashi A, Nishida T, et al. Gain-of-function mutations of platelet-derived growth factor receptor alpha gene in gastrointestinal stromal tumors. *Gastroenterology.* 2003;125:660–7.
7. Sandrasegaran K, Rajesh A, Rushing DA, et al. Gastrointestinal stromal tumors: CT and MRI findings. *Eur Radiol.* 2005;15:1407–14.
8. Ghanem N, Althoefer C, Furtwangler A, et al. Computed tomography in gastrointestinal stromal tumors. *Eur Radiol.* 2003;13:1669–78.
9. Horton KM, Juluru K, Montgomery E, et al. Computed tomography imaging of gastrointestinal stromal tumors with pathology correlation. *J Comput Assist Tomogr.* 2004;28:811–7.
10. Kim HC, Lee JM, Kim SH, et al. Small gastrointestinal stromal tumours with focal areas of low attenuation on CT: pathological correlation. *Clin Radiol.* 2005;60:384–8.
11. Takao H, Yamahira K, Doi I, et al. Gastrointestinal stromal tumor of the retroperitoneum: CT and MR findings. *Eur Radiol.* 2004;14:1926–9.
12. Levy AD, Remotti HE, Thompson WM, Sobin LH, Miettinen M. Gastrointestinal stromal tumors: radiologic features with pathologic correlation. *RadioGraphics.* 2003;23:283–30.
13. Burkill GJ, Badran M, Al-Muderis O, et al. Malignant gastrointestinal stromal tumor: distribution, imaging features, and pattern of metastatic spread. *Radiology.* 2003;226:527–32.

14. Tateishi U, Hasegawa T, Satake M, et al. Gastrointestinal stromal tumor. Correlation of computed tomography findings with tumor grade and mortality. *J Comput Assist Tomogr.* 2003;27:792–8.
15. Yu MH, Lee JM, Baek JH, et al. MRI features of gastrointestinal stromal tumors. *Am J Roentgenol.* 2014;203(5):980–91.
16. Tateishi U, Miyake M, Maeda T, et al. CT and MRI findings in KIT-weak or KIT-negative atypical gastrointestinal stromal tumors. *Eur Radiol.* 2006;16:1537–43.
17. Miyake KK, Nakamoto Y, Mikami Y, et al. The predictive value of preoperative 18F-fluorodeoxyglucose PET for postoperative recurrence in patients with localized primary gastrointestinal stromal tumour. *Eur Radiol.* 2016;26:4664–74.
18. Patnaik S, Jyotsnarani Y, Rammurti S. Radiological features of metastatic gastrointestinal stromal tumor. *J Clin Imaging Sci.* 2012;2:43.
19. Katz SC, Dematteo RP. GISTS and leiomyosarcoma. *J Surg Oncol.* 2008;97:350–9.
20. Kong SH, Yang HK. Surgical treatment of gastric gastrointestinal tumor. *J Gastric Cancer.* 2013;13:3–18.
21. Tashiro T, Hasegawa T, Omatsu M, et al. Gastrointestinal stromal tumor of the stomach showing lymph node metastases. *Histopathology.* 2005;47:438–9.
22. van der Zwan SM, De Matteo RP. Gastrointestinal stromal tumor. 5 years later. *Cancer.* 2005;104:1781–8.
23. Agaimy A, Peter H. Lymph node metastasis in gastrointestinal stromal tumours (GIST) occurs preferentially in young patients ≤ 40 years: an overview based on our case material and the literature. *Langenbeck's Arch Surg.* 2009;394:375.
24. Gong N, Wong CS, Chu YC. Is lymph node metastasis a common feature of gastrointestinal stromal tumor? PET/CT correlation. *Clin Nucl Med.* 2011;36:678–82.
25. Gayed I, Vu T, Iyer R, et al. The role of 18F-FDG PET in staging and early prediction of response to therapy of recurrent gastrointestinal stromal tumors. *J Nucl Med.* 2004;45:17–21.
26. Choi H, Chamsangavej C, Faria SC, et al. Correlation of computed tomography and positron emission tomography in patients with metastatic gastrointestinal stromal tumor treated at a single institution with imatinib mesylate: proposal of new computed tomography response criteria. *J Clin Oncol.* 2007;25:1753–9.
27. Fuster D, Ayuso JR, Poveda A, et al. Value of FDG-PET for monitoring treatment response in patients with advanced GIST refractory to high-dose imatinib. A multicenter GEIS study. *Q J Nucl Med Mol Imaging.* 2011;55:680–7.
28. Prior JO, Montemurro M, Orcurto MV, et al. Early prediction of response to sunitinib after imatinib failure by 18F-fluorodeoxyglucose positron emission tomography in patients with gastrointestinal stromal tumor. *J Clin Oncol.* 2009;27:439–45.